PRESTACK TIME IMAGING ALGORITHM WITH SIMULTANEOUS VELOCITY ESTIMATION IN APPLICATION TO HARD ROCK ENVIRONMENTS

Konstantin Tertyshnikov
DETCRC, Department of Exploration Geophysics, Curtin University
Technology Park West Precinct, ARRC/CSIRO Building, H Block Level 4
26 Dick Perry Ave, Perth WA 6015, Australia
Phone: 8 9266 3519
Facsimile: 8 9266 3407
E-mail: k.tertyshnikov@postgrad.curtin.edu.au

Andrej Bóna
DETCRC, Department of Exploration Geophysics, Curtin University
Technology Park West Precinct, ARRC/CSIRO Building, H Block Level 4
26 Dick Perry Ave, Perth WA 6015, Australia
E-mail: a.bona@curtin.edu.au

Roman Pevzner
DETCRC, Department of Exploration Geophysics, Curtin University
Technology Park West Precinct, ARRC/CSIRO Building, H Block Level 4
26 Dick Perry Ave, Perth WA 6015, Australia
E-mail: r.pevzner@curtin.edu.au

Date: April 20, 2015

ABSTRACT

Reflection seismic imaging faces a number of difficulties in hard rock environments. One of them is the estimation of the propagation velocity of seismic waves. Therefore, Imaging algorithms that do not require prior construction of a velocity model seem promising for such environments. In this paper we illustrate an application of prestack time migration, which does not require an input velocity model, to hard rock conditions, and we demonstrate its effectiveness on synthetic data. This approach is based on an estimation of local event slopes (horizontal slownesses) in common-shot and common-receiver gathers and a subsequent calculation of the migration attributes (migration velocity, vertical travel-time and horizontal coordinates of the migrated reflection point). These attributes allow us to derive all the information needed to construct a time migrated image. We also use the obtained migration velocities as an input velocity model for Kirchhoff prestack time migration (PSTM) and compare the results of the proposed approach with a conventional Kirchhoff migration using as an input the picked NMO velocity model. This application to a hard rock synthetic model illustrates the potential of the presented migration algorithm for imaging in hard rock seismic exploration. We believe that this approach can be used in hard rock seismic processing workflows as an automatic tool to obtain an input velocity model for the Kirchhoff PSTM.

Key Words: seismic, imaging, prestack, migration, hard rock.

INTRODUCTION

A velocity model for the subsurface is an essential component in most conventional seismic migration algorithms. However, velocity information is often unavailable, and obtaining this information from the seismic data itself may be a difficult task. This is often the case in hard rock environments, which include complex faults, fracture zones, steep dips and rock alterations. Additionally, this type of environment is often characterized by low reflectivity and high ambient noise, since most of the seismic exploration for minerals is conducted across "brown" fields, in an attempt to define extensions of existing mineralizations. Consequently, defining a velocity field over sub-vertical structures and complex, fractal boundaries with intrinsically low signal-to-noise ratio and lack of borehole information is difficult and alternative data processing strategies need to be employed. For such situations, imaging methods that do not require an input velocity model are desirable.

In the past few decades, many researchers have published results from velocity-independent seismic time migration techniques. The majority of these imaging approaches are based on the evaluation of the local dips of seismic events (horizontal slownesses). A number of papers that discuss the use of slownesses for constructing velocity independent imaging have been published during the last 75 years. The concept of controlled directional sensitivity, e.g. estimating local slopes from pre-stack data and using them to estimate migration velocities and locations, first appeared in Rieber (1936) and Riabinkin (1957). Sword Jr (1987) summarizes these concepts as a method of controlled directional reception. The idea of velocity independent imaging for the migration of horizontal reflectors was suggested in a paper by Ottolini (1983b); he presented a method for building the image by applying the time dips of the seismic data at every point on the registered data. Fomel (2007) expanded Ottolini's concept; he used information about local event slopes from common-midpoint and

common-offset domains to obtain the complete reflection geometry. Cooke et al. (2009) used horizontal slownesses not only to perform time imaging and estimation of velocities, but also for the suppression of multiplies. Bona (2009) presented a velocity-less prestack time imaging algorithm, where only one (common-shot or common-receiver) domain is required; however he needed to calculate both the first and second derivatives of the travel-time.

In this paper we apply the method of controlled directional reception to a synthetic dataset simulating a hard rock environment. This prestack time migration algorithm does not require an initial velocity model. The presented algorithm is based on an estimation of horizontal slownesses (local event slopes) that are used to produce the migration attributes (the location of the migrated events as well as the migration velocities). The calculated attributes allow us to map seismic amplitudes from the prestack data domain into the time migrated image.

We analyse the presented prestack time migration based on the assumption of hyperbolic offset-traveltime curves. We test the imaging algorithm on some simple models with one dipping interface and a syncline boundary. To illustrate the potential of the method for hard rock environments, we show the imaging results from a complex 2D hard rock geological model and compare them with the conventional Kirchhoff prestack time migration.

MIGRATION ALGORITHM AND IMPLEMENTATION

In this paper we discuss an application of the method of controlled directional reception, a prestack time migration technique which is based on estimation of local event slopes for common-shot and common-receiver domains and obtaining the values of attributes: migration velocity (V), vertical travel-time (t_0) and horizontal coordinate of the migrated reflection point (x_m). Herein we use equations for these parameters that were derived for 2D geometry

by Cooke et al. (2009) from the travel-time equation (double-square-root equation) for reflections in effective homogeneous media.

$$x_m = x_s - (x_r - x_s)p_s \frac{t-(x_r-x_s)p_r}{t(p_r-p_s)+2(x_r-x_s)p_s p_r}, \qquad (1)$$

$$V^2 = \frac{x_s-x_m}{tp_s} + \frac{x_r-x_m}{tp_r}, \qquad (2)$$

$$t_0 = \frac{|x_s-x_m|}{V}\frac{\sqrt{\frac{1}{V^2}-p_s^2}}{|p_s|}, \qquad (3)$$

Here, p_r and p_s are values of horizontal slownesses measured in common-shot and common-receiver gathers respectively; x_s and x_r are the locations of source and receiver; t is the travel-time of the migrated event. The equations (1) – (3) represent a system of three equations with three unknown migration attributes. For every event in the time domain, the travel-time and locations of shots and receivers are known, and p_r and p_s can be derived from seismic data. The solution of the presented system allows us to obtain the velocity model and at the same time the output migration locations t_0 and x_m for every sample from the input dataset. As a result, every amplitude of each trace from the input dataset has a definite pair of image coordinates t_0 and x_m. To create the final result we add every single input amplitude sample onto a single point of the migrated image using the coordinates given by expressions (1) and (3). In contrast to the Kirchhoff prestack time imaging, the reflection amplitude is not distributed over an ellipse defined by velocity and geometry; instead it is mapped directly onto the calculated image point. Thus, we are not including amplitude and phase corrections

(Yilmaz, 2001), which account for the angle dependence of amplitudes (obliquity factor), spherical spreading, and wavelet shaping.

In the special case of a local slopes equal to zero we have derived the equations for the migration attributes from geometrical considerations. When p_s approaches zero, the attributes can be computed from the following system:

$$x_m = x_s,\ V^2 = \frac{2d}{tp_r} - \frac{d^2}{t^2},\ t_0 = \frac{V^2t^2 - d^2}{2tV^2} \qquad (4)$$

When p_r is equal to zero, the migration parameters are obtained from the following equations:

$$x_m = x_r,\ V^2 = -\frac{2d}{tp_r} + \frac{d^2}{t^2},\ t_0 = \frac{V^2t^2 - d^2}{2tV^2} \qquad (5)$$

The method is not designed to handle the case of both local slopes p_r and p_s approaching the same value, which corresponds to the zero offset case; the zero-offset data are excluded from the migration process. When p_r and p_s are taking the equal values, there is not enough information to recover the location of the reflection point.

A good estimation of the values of horizontal slownesses p_r and p_s is necessary for this migration algorithm. It is important to note that the horizontal slowness is determined in the pre-stack domain as a component of a normal vector to the tangent plane of the travel-time surfaces; they could be derived from CMP and offset coordinates rather than source and receiver locations (Harlan and Claerbout, 1996; Fomel, 2007). There are a number of techniques used to calculate the local event slopes for every point in the seismic dataset. Ottolini (1983a) suggested the local slant stack method; Fomel (2002) described an extension to a plane-wave destruction algorithm of Claerbout (1992); Schleicher et al. (2009) further extended the method of plane-wave destructors. The algorithm that we selected is based on a

semblance analysis (Neidell and Taner, 1971) of local slant stacks (Ottolini, 1983a; Harlan et al., 1984) . This algorithm gives us the most stable and robust data for determining local event slopes.

The horizontal slownesses p_s and p_r are computed as the spatial components of a normal vector to the tangent plane of the travel-time surfaces. In particular, the algorithm is implemented as follows. For every trace we select the neighbouring traces within a certain radius in the shot-receiver space. Then for each pair of local slopes p_s and p_r from a specified range, we compute the corresponding time shifts for each of the selected traces and calculate the semblance of the time-shifted traces in a chosen running time window. For each sample we find the slopes corresponding to the maximum semblance. These slopes correspond to the values of slownesses in common-shot and common-receiver gathers p_s and p_r. The described implementation allows any 2D geometry. Prior to migration of the input sample onto the final image we sum the traces along the estimated local slopes to increase signal to noise ratio.

For geometries with conflicting dips, the algorithm selects the dip that corresponds to the maximum of the estimated semblance. The values of p_r and p_s are always associated with the same dipping event because they are projections of the same normal vector on the fitted tangent plane (this might not be the case if we estimate p_r and p_s independently).

EXAMPLE 1: BASIC MODELS

The presented velocity-independent imaging algorithm was tested on several 2D synthetic models of varying complexity. First, to test the accuracy of the algorithm, we applied the migration to two convolution models: a dipping reflector and a syncline model with constant velocities.

The results of the migration for data from a dipping reflector are shown in Figure 1. The dipping angle of the reflection interface was 20°. To construct the seismograms, we convolved a zero-phase, 30 Hz dominant frequency wavelet with spike-traces of unit amplitude. The shot-gathers were calculated for two hundred receivers and shots using a ray-tracing method; the spacing between both receiver and shot positions was 10 m; shots were located in the same position as the receivers. The velocity of the upper medium was 3000 m/s. We computed one-second long seismic traces. As noted above, the horizontal slownesses were estimated by using semblance. Using these values of the horizontal slownesses and the arrival time of each sample, the migration attributes (velocity (V), vertical travel-time (t_0) and horizontal coordinate (x_m)) were calculated. The attributes t_0 and x_m define the location of migrated data; each sample was placed in the final image in accordance with these two parameters. The real position of the dipping interface in time domain is shown in Figure 1a.

We applied the proposed algorithm to two cases: noise-free seismograms and gathers containing a noise level of 30%. The random noise was added to the spike-traces before convolution with the wavelet, resulting in noisy data with the same frequency range as the noise-free data. An example of the seismogram containing a noise level of 30% is shown in Figure 2a. An example of the distribution of semblance maxima, which is used for the local slopes computation, is shown in Figure 2b. The p_r- and p_s-values for a shot gather of noisy data are shown in Figure 2c and 2d respectively.

We plot the migrated section of the dipping interface from the noise-free data in Figure 1b; in this case we extracted the local event slopes using a radius of 25 m that gave us up to 21 traces to analyse in the spatial dimension and a 5 sample window in the temporal direction. Figure 1c shows the migration result of the dipping interface from noisy data. In this example, to estimate the horizontal slownesses we utilized the same parameters for the spatial

and temporal dimensions (up to 21 traces and 5 time samples). The migrated section of the dipping interface from the noise-free data is clearly imaged; the slope and position of the interface are the same as on the true model section. The image from the noisy data is slightly blurred, but the dip and position of the boundary were recovered correctly. To enhance the image quality we increased the number of traces in a group up to 177 (radius 75 m) and enlarged the time window up to 15 samples. Figure 1d shows the migration result from noisy data with expanded spatial and temporal estimation parameters. The utilization of the larger windows allowed us to obtain a clear image from the noisy seismograms. The lower part of the interface was not plotted on the final images in all cases, because there were no geophones in the presented geometry setup and therefore no reflection energy from that area. Figure 3 illustrates the results for data from a syncline model. We used the same geometry setup to obtain the seismograms for the fold model. The velocity of the upper medium was 3000 m/s. The parameters of the wavelet and spike-traces were similar to those in the previous example. We also modelled two cases– without noise and 30% noise. The actual position of the syncline in the time domain is shown in Figure 3a. To extract the horizontal slownesses from the noise-free data, we applied the same parameters (25 m radius and a 5 sample time window), for the noisy data we also examined two setups similar to the previous model. Figure 3b shows the migration result from noise-free gathers. Figures 3c and 3d show the migrated images from two noisy cases respectively. On the migrated images of the syncline, the amplitude distribution along an interface is uneven. This can be explained by the various amount of energy (fold) that is reflected from different parts of the model, not by errors in dip estimations. The depth of the fold and the slopes of its sides match the actual model. The application of larger windows helped to recover the syncline shape completely, and it is correctly located. Figure 3e shows the velocity distribution obtained from the noisy data using a radius of 75m and 15 time samples to estimate the slopes. We show only the

velocities at locations to which more than 15 samples contribute from different input traces. The velocities correspond to the velocity above the reflector, 3000 m/s. Figure 3f shows the distribution of the reflected energy from the spike syncline model (unit amplitude along the interface). The number of points coming from the input data to a certain location on the migrated image is shown. To produce this picture we used a unit amplitude model and true local slopes. It is clearly seen that different amount of energy is coming from the syncline's interface.

The results of the migration for both models are sufficiently promising for seismic applications. The slope dependant summation and tuning the searching parameters for slownesses estimation can significantly improve the quality of the final image. The accuracy of estimation of the local event slopes, and as a result, the quality of the final image, depends on the quality and coherency of the input data.

EXAMPLE 2: SYNTHETIC DATASET BASED ON REALISTIC GEOLOGICAL MODEL

Here we apply the presented prestack time migration to synthetic data generated by a finite-difference method using TesseralCS-2D modelling software (a model that simulates real geological conditions). This model is based on the geology of the Sunrise Dam – Cleo gold deposit in Western Australia (Brown et al., 2002). The Sunrise Dam operation is about 55 km south of Laverton, 220 km NNE of Kalgoorlie, and 770 km NE of Perth, in the Eastern Goldfields province of the Yilgarn Craton. The constructed model is shown in Figure 4. The host rocks are represented by volcaniclastic formations overlain by a variable depth slow velocity regolith. The model has shallow to steep dipping shear zones, mafic and felsic intrusions, interbedded dolerite, and Banded Iron Formations (BIFs). The main gold mineralization is confined to shear zones and to high grade discrete quartz carbonate narrow veins. There are spatial correlations between felsic porphyry dikes and gold mineralization

lodes. The porphyry dikes and their margins preferentially control the location of these zones, and they are parallel to the porphyry dike. Ore zones are best developed within BIFs and are characterized by pyrite replacement of magnetite-rich layers (Brown et al., 2002).

Hard rock seismic exploration in Western Australia is still not widespread and there is a limited knowledge of seismic and sonic velocities in the area. P-wave velocities (Table 1) were approximated from RMS stacking velocities used in the reprocessing of the Anglo Gold Ashanti regional seismic line which passed over part of the Sunrise Dam deposit (Urosevic and Evans, 2007). In some cases velocities and densities were obtained from the literature (Telford et al., 1990) or selected from a TesseralCS-2D parameter menu for corresponding rock types. This menu has a library of minimum, average and maximum elastic parameters for common sedimentary, metamorphic and igneous rock types. The values of the velocity and density for every unit are represented in Table 1.

A total number of 181 receiver locations along the surface were used, the distance between the receivers was 5 m; shots were located at the same positions as the receivers. A Ricker wavelet with a central frequency of 80 Hz was chosen as the source signal. Acoustic full-waveform modelling was used to obtain synthetic seismograms. The sampling rate was 0.5 ms and the record length was 1 second. To compare the actual locations of the geological features and the targets of the model with the final results of the time migration, we converted the velocity model to time domain, as shown in Figure 5. The RMS velocities of the hard rock model were computed from the depth velocity distribution and are shown in Figure 6.

No pre-processing was applied to the synthetic seismograms prior to the imaging step using the migration algorithm. The velocity analysis and mapping of the amplitudes to the final image are part of the same process. This allows us to avoid manually processing the velocity

model estimation and makes the migration automated. Figure 7 shows the smoothed section of migration velocities obtained by the algorithm; in the case when multiple points contribute to the same location from different input traces, a weighted average is used in the final velocity model; the range of migration velocities corresponds to the actual velocity distribution.

The final migrated section of the 2D geological synthetic model is presented in Figure 8. The amplitudes of the dataset were collected and summed into the image according to the corresponding values of the attributes: vertical travel-time and horizontal reflection point location. Figure 9 illustrates the migrated image overlaid on the true velocity model. The interface between regolith and volcaniclastic rocks is displayed very clearly. The top of the mafic intrusion can be distinguished easily; the steep sides of this intrusion are not visible, because most of the reflected energy is not recorded by the receivers. The whole felsic porphyry body is distinctly observed. The shear zones can also be traced on the migrated section. We can see that all the main geological targets, which are correlated with the gold mineralization zones (the felsic dyke and shear zones), can be clearly identified on the final image.

The next step of the study was to compare the result of the presented prestack time migration algorithm with a conventional Kirchhoff prestack time migration (PSTM). The migration velocities, which were obtained during the migration process, were used as an input velocity model for the Kirchhoff PSTM. The PSTM stack section is shown in Figure 10. The comparison of the Kirchhoff migration result with the actual model is presented in Figure 11. Both final migration images (Figure 8 and Figure 10) are comparable in terms of showing the main features and structures of the geological section. The Kirchhoff migrated image appears to be more continuous in several locations; the top of the banded iron formation is clearly

imaged on the PSTM section. We conclude that the final migrated section from the presented algorithm is of reasonable quality and that this approach can be used in a hard rock seismic processing workflow as an automatic tool to obtain an input velocity model for the Kirchhoff PSTM.

Lastly, we performed conventional processing of the synthetic data to obtain the stacking velocities. The velocity analysis was done after applying DMO corrections in Promax processing software; a section of the obtained stacking velocities is shown in Figure 12. This velocity model was then used as an input model for the Kirchhoff PSTM; the result of that migration is shown in Figure 13. Comparing Figure 13 with Figure 10 shows that the results of both Kirchhoff migration sections are almost identical. Figure 14 shows an overlap of the PSTM image and the actual model. The migrated section with the stacking velocities clearly indicates the interfaces and features of the geological model. We can conclude that the migration velocities resulting from the proposed imaging process can be successfully used as an input velocity model for conventional migration techniques. The initial velocity analysis routine can be excluded from the processing flow. Such a modified workflow should be useful for hard rock seismic exploration, because in these environments the velocity spectra are usually incoherent and it is difficult to obtain an appropriate velocity model.

DISCUSSION

We tested the presented prestack time migration on several synthetic examples to assess the potential of applying this imaging technique to hard rock seismic exploration. The presented algorithm estimates the local slopes in common-shot and common-receiver domains using an assumption of hyperbolic offset-traveltime curves (Cooke et al., 2009). This assumes hyperbolic reflection responses; a deviation from this assumption could cause errors in the estimation of migration attributes. The horizontal slownesses contain comprehensive

information about the geometry of reflections. These local event slopes allow us to calculate migration velocities, vertical travel-time and horizontal coordinates of the migrated locations for every input sample of the prestack data and directly map the events into the time-migrated image. The accuracy of the final migrated images strongly depends on the quality of estimation of the horizontal slownesses. Among the several possible approaches, we chose a semblance approach to obtain the local slopes, as it provides the most stable and robust results. Nevertheless, as was shown on the convolution examples, the accuracy of this estimation largely depends on the coherency and quality of the input data, but can be enhanced by appropriate choice of the searching parameters. The quality of the final images can be improved by summation along the obtained local slopes.

Computationally, this imaging technique is relatively fast. The most time consuming part is the estimation of the local slopes of the seismic events, which is dependent on the used method. Mapping the seismic events from the input data to the migrated section goes in parallel with attributes calculation and amplitude–phase corrections; this procedure is almost instantaneous in comparison with slope estimation. Also, this migration avoids the manual velocity analysis process. Moreover there is a possibility of progressively building the velocity field and migration image in real time, particularly for certain 2D seismic geometry setups.

The application of velocity-independent migration algorithms is especially important to hard rock seismic exploration in areas with high velocity and complex structures. To use the presented prestack time migration effectively in hard rock environments, we need to test it on a number of real seismic datasets from different geological regions and compare it to other imaging techniques.

CONCLUSIONS

We have presented an application of a prestack time migration algorithm based on the method of controlled directional reception to 2D geological synthetic models. This algorithm was successfully tested on simple synthetic models. Applying it to a complex 2D geological model has shown that proposed prestack time imaging is stable and produces satisfactory results. All the main features and structures of the hard rock geological section can be clearly distinguished on the migrated image. The presented prestack time migration has a number of benefits. The main benefit is that no input velocity model is required. This is important especially for hard rock sites, where information about velocities is often incomplete. In fact, a reasonably accurate velocity model is derived during the migration process. An additional benefit is that the estimated velocity model can be used as input for conventional migration techniques.

As part of future development, we intend to improve the implementation of the presented algorithm in terms of accuracy of estimation of the local event slopes by including quality control of the slope estimation based on the semblance value. Further improvements are possible by considering the migration of the events not to a single location. This could be achieved by spreading them over the first Fresnel zone along the estimated dipping interface, or by using Gaussian beams.

ACKNOWLEDGMENTS

The research is carried out at Curtin University at the Department of Exploration Geophysics. The work has been supported by the Deep Exploration Technologies Cooperative Research Centre whose activities are funded by the Australian Government's Cooperative Research Centre Programme. This is DET CRC Document 2013/144. We would like to thank Andrew

Greenwood for the hard rock model. We are also grateful to Aleksei Shevchenko for constructive discussions about the method of controlled directional reception.

REFERENCES

Bona, A., 2009, Velocityless migration of source gathers: *SEG Technical Program Expanded Abstracts*, **28(1)**, 3000-3004.

Brown, S., Groves, D. and Newton, P., 2002, Geological setting and mineralization model for the Cleo gold deposit, Eastern Goldfields Province, Western Australia: *Mineralium Deposita*, **37(8)**, 704-721.

Claerbout, J.F., 1992, *Earth soundings analysis: Processing versus inversion:* 6, Blackwell Scientific Publications.

Cooke, D., Bona, A. and Hansen, B., 2009, Simultaneous time imaging, velocity estimation, and multiple suppression using local event slopes: *Geophysics*, **74(6),** WCA65-WCA73.

Fomel, S., 2002, Applications of plane-wave destruction filters: *Geophysics*, **67(6)**, 1946-1960.

Fomel, S., 2007, Velocity-independent time-domain seismic imaging using local event slopes: *Geophysics,* **72(3),** S139-S147.

Harlan, W. and Claerbout, J., 1996, Tieman's conversion of common-midpoint slant stacks to common-source: *SEP-92, Stanford Exploration Project,* 293-298.

Harlan, W., Claerbout, J. and Rocca, F., 1984, Signal/noise separation and velocity estimation: *Geophysics*, **49**, 1869-1880.

Neidell, N.S. and Taner, M.T., 1971, Semblance and other coherency measures for multichannel data: *Geophysics*, **36(3)**, 482-497.

Ottolini, R., 1983a, Signal/noise separation in dip space: *SEP-37, Stanford Exploration Project,* 143 - 149.

Ottolini, R., 1983b, Velocity independent seismic imaging: *SEP-37, Stanford Exploration Project,* 59 - 68.

Riabinkin, L.A., 1957, Fundamentals of resolving power of controlled directional reception (CDR) of seismic waves: *in L. Lu, ed., Slant-stack processing, 1991, SEG,* P36–P60.

Rieber, F., 1936, A new reflections system with controlled directional sensitivity: *Geophysics,* **1(1)**, 97-106.

Schleicher, J., Costa, J.C., Santos, L.T., Novais, A. and Tygel, M., 2009, On the estimation of local slopes: *Geophysics,* **74(4)**, P25-P33.

Sword Jr, C.H., 1987, Tomographic determination of interval velocities from reflection seismic data: The method of controlled directional reception: *Stanford University*.

Telford, W.M., Geldart, L.P. and Sheriff, R.E., 1990, *Applied geophysics:* Cambridge Univ Pr.

Urosevic, M. and Evans, B., 2007, Feasibility of seismic methods for imaging gold deposits in Western Australia: *Minerals and Energy Research Institute of Western Australia*.

Yilmaz, Ö., 2001, *Seismic data analysis:* Society of Exploration Geophysicists.

TABLES

Table 1: Velocity-Density table for the 2D geology model.

#	Rock Unit	Vp m/s	Density (kg/m^3)
A	Regolith	2200	2000
B	Volcaniclastic	5500	2800
C	Mafic intrusion	6200	3500
D	Banded Iron Formation	6200	2750
E	Dolerite	6400	2900
F	Felsic Porphyry	6700	3100
G	Fault	5800	2650
H	Shear Zone	5000	2600

FIGURES AND IMAGES

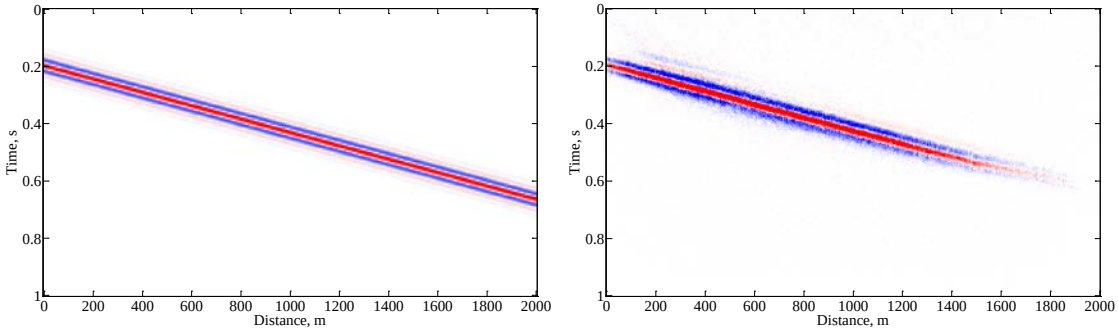

a. True position of an interface in time.

c. Migrated image of data with 30% noise level (25m radius and 5 time samples window for slopes estimation).

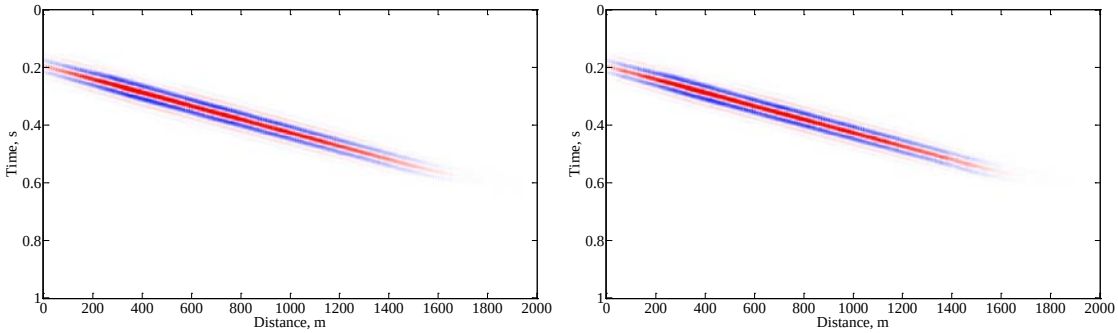

b. Migrated image of noise-free data.

d. Migrated image of data with 30% noise level (75m radius and 15 time samples window for slopes estimation).

Fig. 1. Convolution model of a dipping interface. a) true position of a dipping interface in time scale. b) migrated image of an interface of noise-free data (25m radius and 5 time samples window for slopes estimation). c) migrated image of an interface of data with 30% noise level (25m radius and 5 time samples window for slopes estimation). d) migrated image of an interface of data with 30% noise level (75m radius and 15 time samples window for slopes estimation).

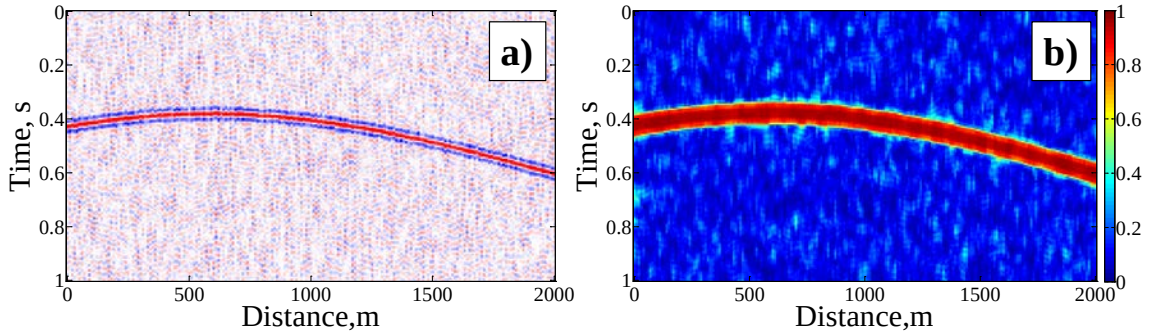

a. Shot-gather at 1000 m (data with 30% noise level).

b. Semblance panel for the shot-gather at 1000 m (data with 30% noise level).

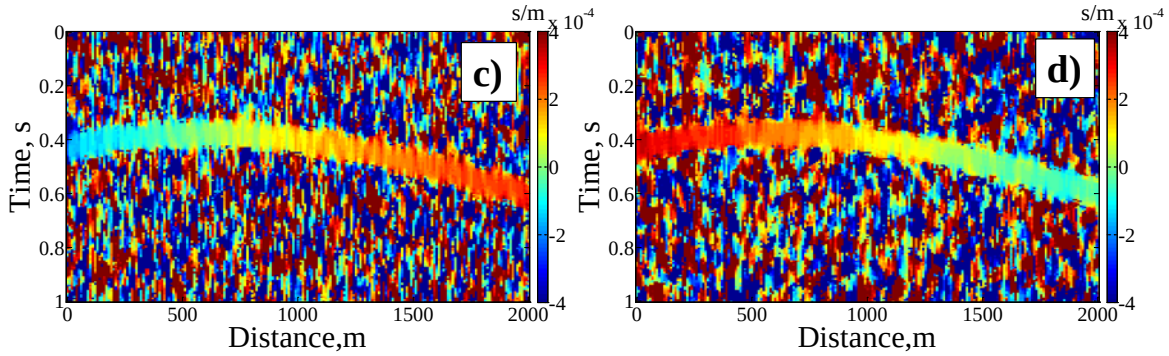

c. Shown p_r – values for the shot-gather at 1000 m (data with 30% noise level).

d. Shown p_s – values for the shot-gather at 1000 m (data with 30% noise level).

Fig. 2. Convolution model of a dipping interface of data with 30% noise level. a) Example of a shot gather at 1000 m. b) Shown the semblance panel for the shot gather at 1000 m. c) Shown p_r – values for the shot gather at 1000 m. d) Shown p_s – values for the shot gather at 1000 m. (25 m radius and 5 time samples window for slopes estimation).

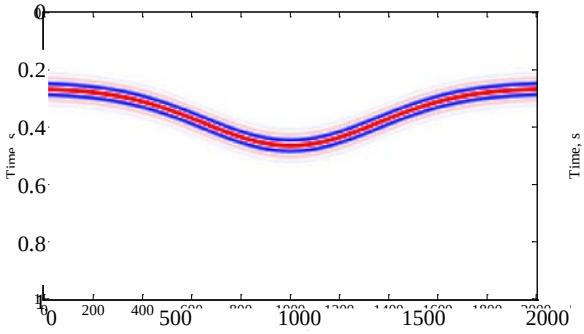

a. True position of a syncline in time.

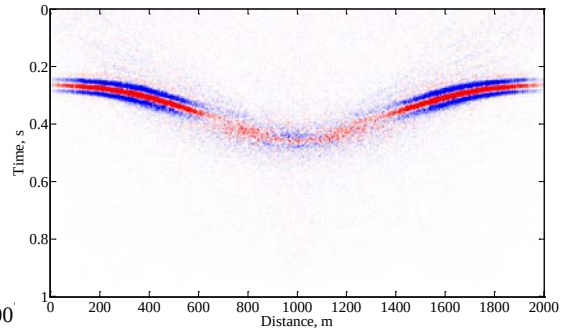

c. Migrated image of data with 30% noise level (25m radius and 5 time samples window for slopes estimation).

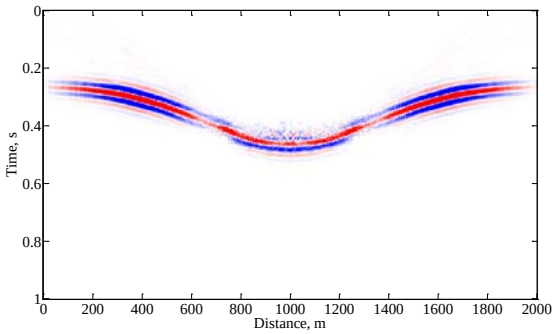

b. Migrated image of noise-free data.

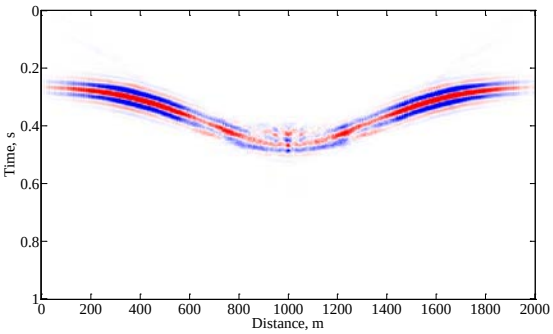

d. Migrated image of data with 30% noise level (75m radius and 15 time samples window for slopes estimation).

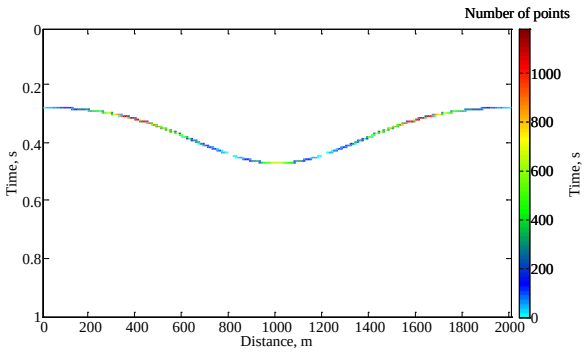

f. Energy distribution from the unit amplitude syncline model. True slopes were used for the migration.

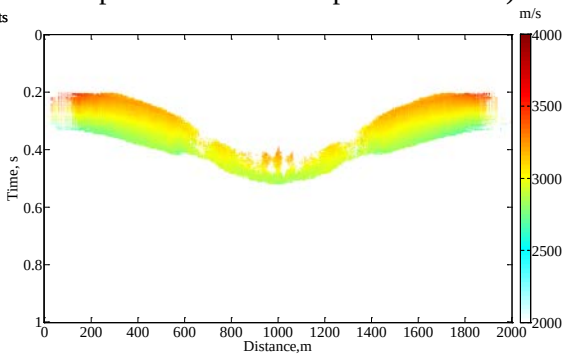

e. Velocity distribution along the syncline for the case (d).

Fig. 3. Convolution model of a syncline. a) true position of a syncline in time scale. b) migrated image of a syncline of noise-free data (25m radius and 5 time samples window for slopes estimation). c) migrated image of a syncline of data with 30% noise level (25m radius and 5 time samples window for slopes estimation). d) migrated image of a syncline of data with 30% noise level (75m radius and 15 time samples window for slopes estimation). e)

velocity distribution along the syncline for the case (d) (shown only velocities at locations to which more then 15 samples contribute from different input traces). f) Energy distribution from the unit amplitude syncline model. Figure shows how many points are migrated to a given location on the image. True analytically computed slopes were used for the migration. The energy distribution corresponds to the strenght of the migrated data in subfigure (b).

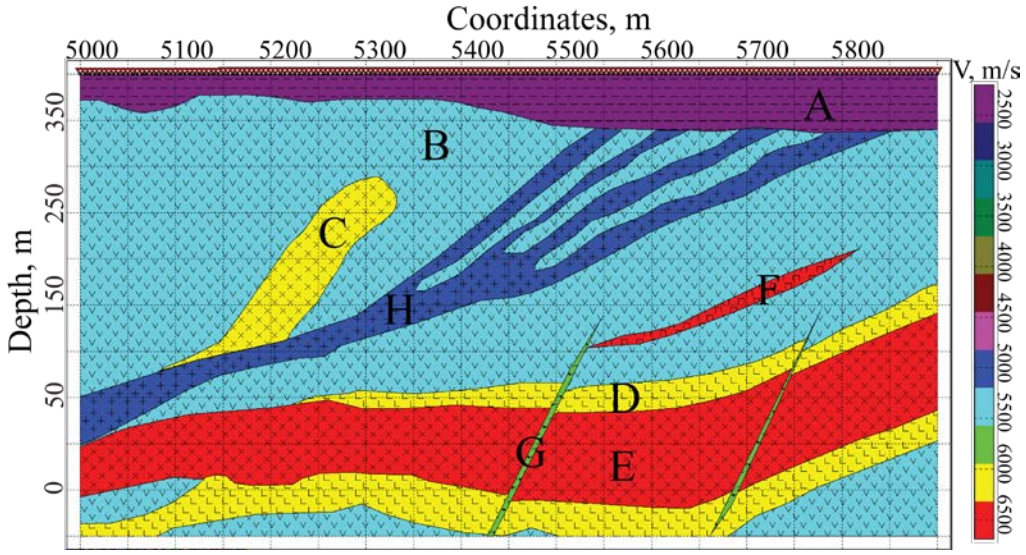

Fig. 4. 2D hard rock velocity model, which was used to generate a synthetic seismic dataset.

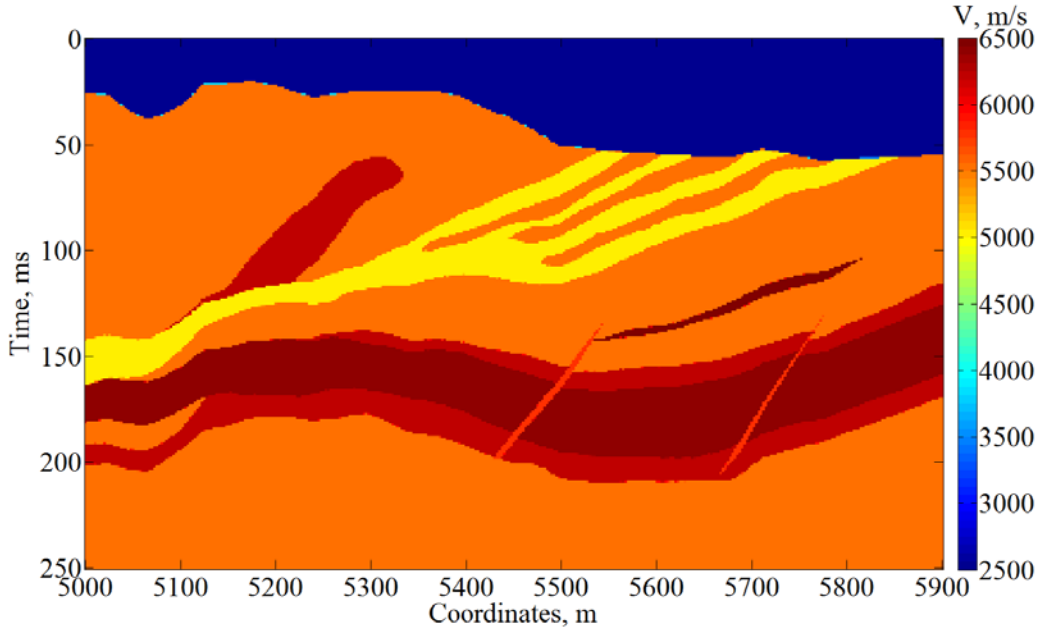

Fig. 5. 2D hard rock velocity model converted in time domain.

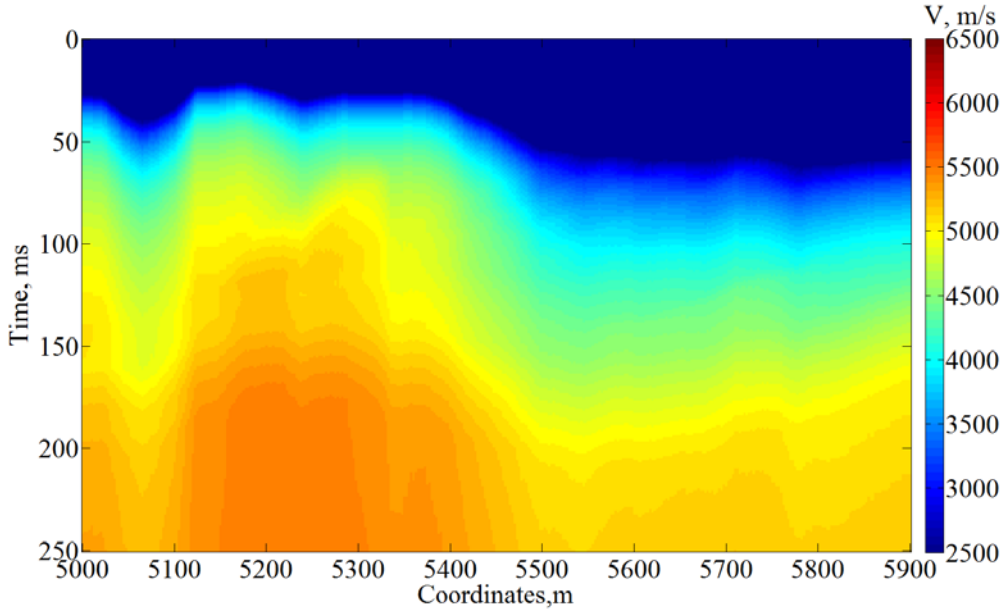

Fig. 6. Section of the RMS velocities.

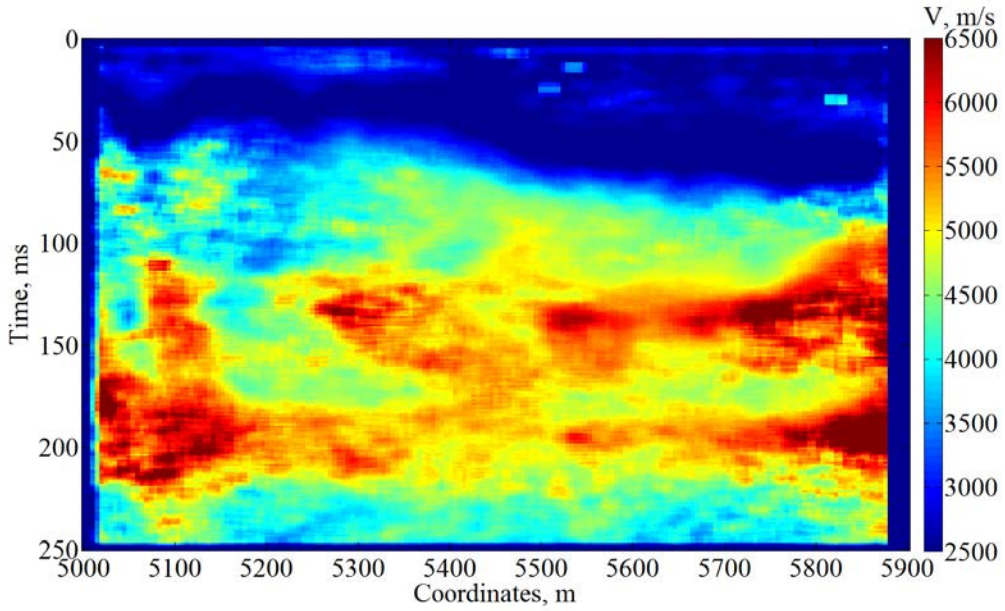

Fig. 7. Section of the migration velocities.

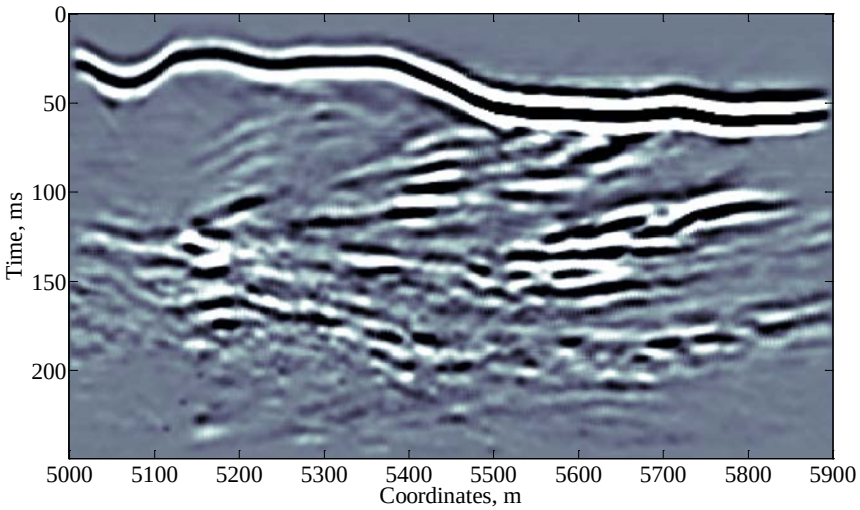

Fig. 8. The final image of the prestack time migration from the 2D hard rock geology model.

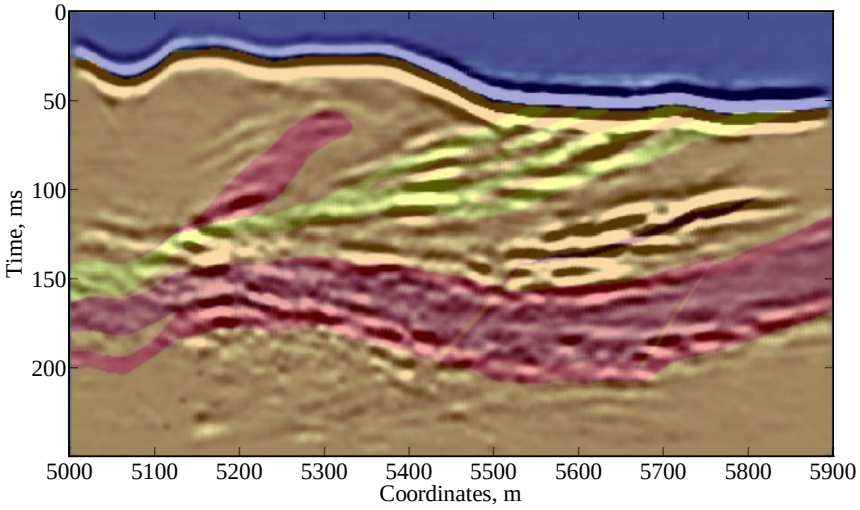

Fig. 9. The prestack migration image from the 2D hard rock geology model. Actual velocity model is overlaid onto the migrated section.

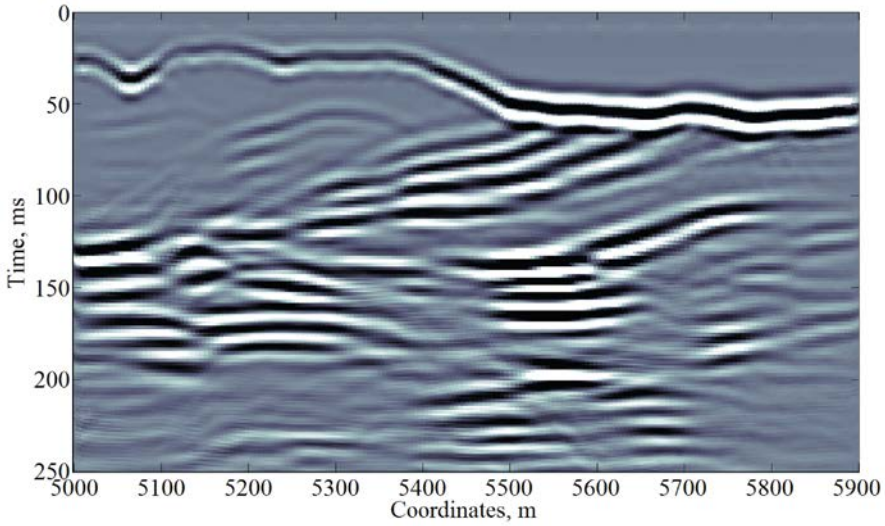

Fig. 10. Kirchhoff PSTM image from the 2D hard rock synthetic model. Migration velocities from the presented migration were used as an input velocity model.

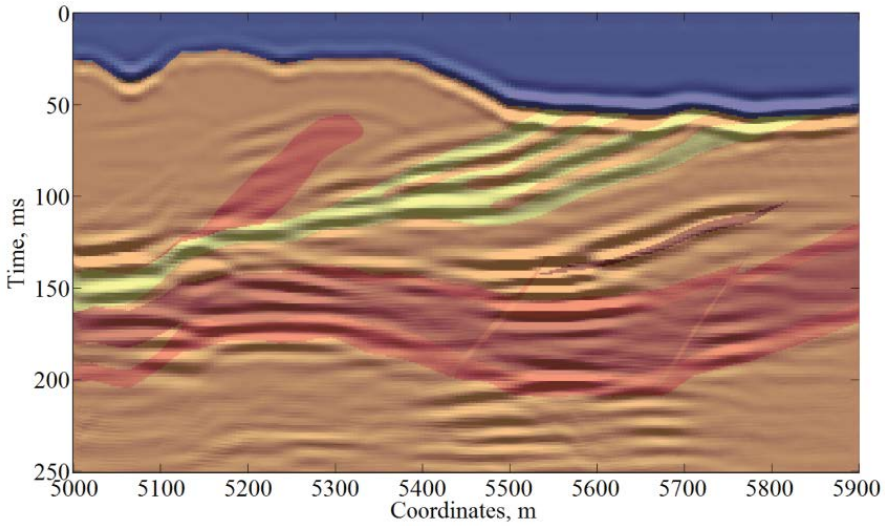

Fig. 11. Kirchhoff PSTM image from the 2D hard rock synthetic model. Migration velocities from the presented migration were used as an input velocity model. Actual velocity model is overlaid onto the migrated section.

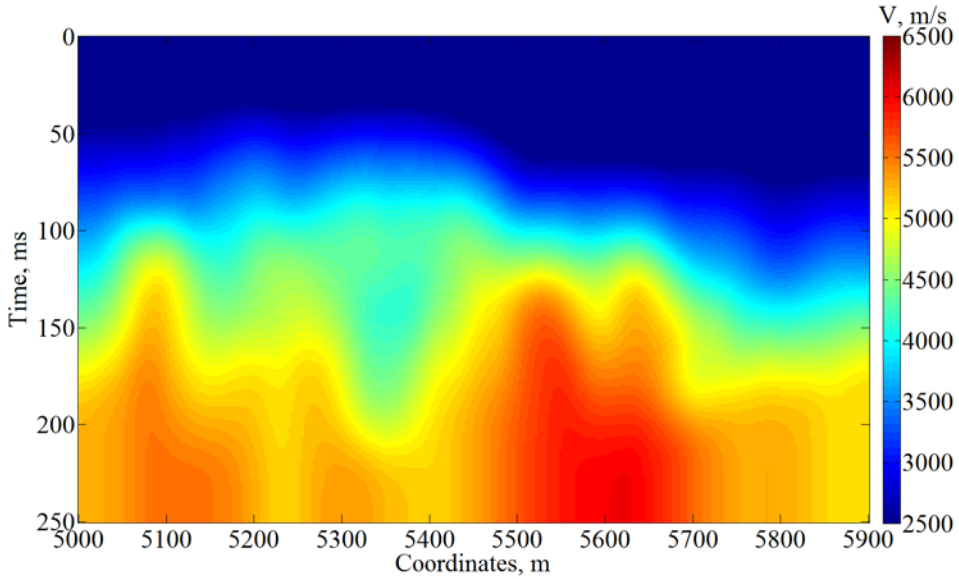

Fig. 12. 2D stacking velocity model, which was obtained from a velocity analysis after applying DMO corrections.

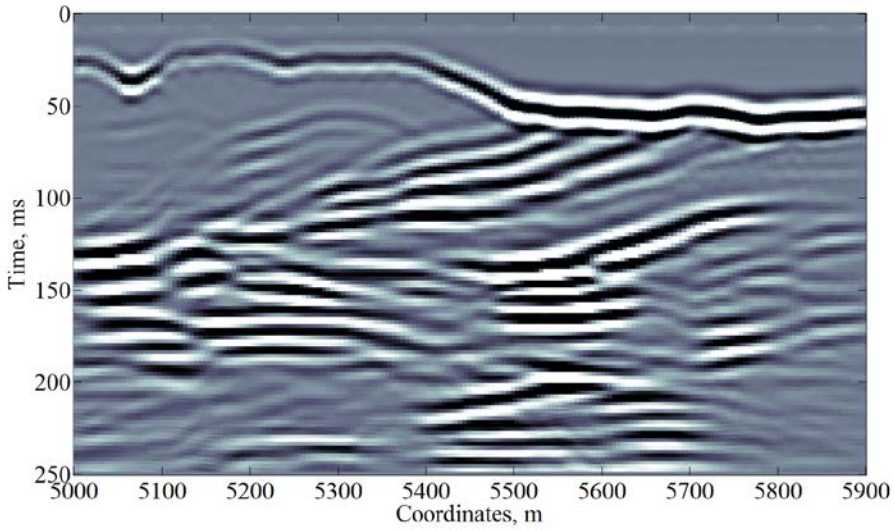

Fig. 13. Kirchhoff PSTM image from the 2D hard rock synthetic model. Stacking velocities from the velocity analysis were used as an input velocity model.

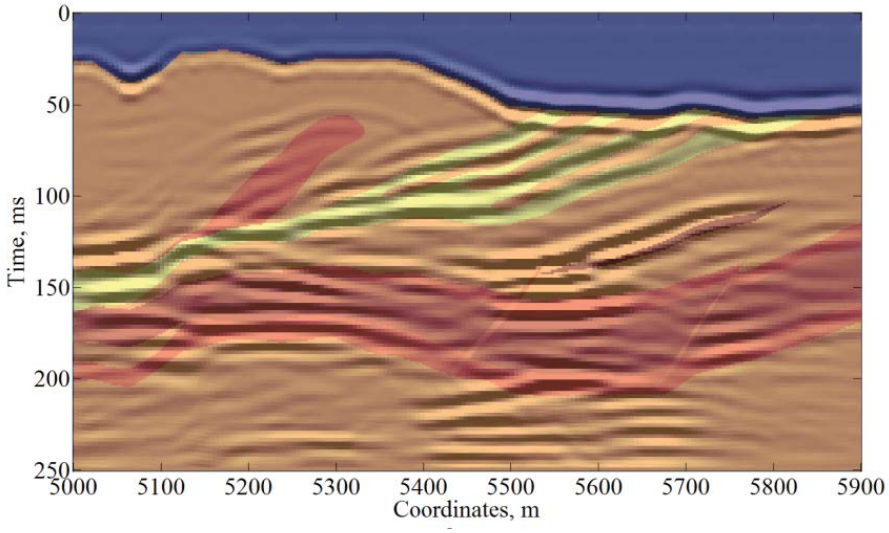

Fig. 14. Kirchhoff PSTM image from the 2D hard rock synthetic model. Stacking velocities from the velocity analysis were used as an input velocity model. Actual velocity model is overlaid onto the migrated section.

FIGURE CAPTIONS

Fig. 1:

Convolution model of a dipping interface. a) true position of a dipping interface in time scale. b) migrated image of an interface of noise-free data (25m radius and 5 time samples window for slopes estimation). c) migrated image of an interface of data with 30% noise level (25m radius and 5 time samples window for slopes estimation). d) migrated image of an interface of data with 30% noise level (75m radius and 15 time samples window for slopes estimation).

Fig. 2:

Convolution model of a dipping interface of data with 30% noise level. a) Example of a shot gather at 1000 m. b) Shown the semblance panel for the shot gather at 1000 m. c) Shown p_r – values for the shot gather at 1000 m. d) Shown p_s – values for the shot gather at 1000 m. (25 m radius and 5 time samples window for slopes estimation).

Fig. 3:

Convolution model of a syncline. a) true position of a syncline in time scale. b) migrated image of a syncline of noise-free data (25m radius and 5 time samples window for slopes estimation). c) migrated image of a syncline of data with 30% noise level (25m radius and 5 time samples window for slopes estimation). d) migrated image of a syncline of data with 30% noise level (75m radius and 15 time samples window for slopes estimation). e) velocity distribution along the syncline for the case (d) (shown only velocities at locations to which more then 15 samples contribute from different input traces). f) Energy distribution from the

unit amplitude syncline model. Shown how many points are coming from the input data to a certain location on the image. True slopes were used for the migration.

Fig. 4:

2D hard rock velocity model, which was used to generate a synthetic seismic dataset.

Fig. 5:

2D hard rock velocity model converted in time domain.

Fig. 6:

Section of the RMS velocities.

Fig. 7:

Section of the migration velocities.

Fig. 8:

The final image of the prestack time migration from the 2D hard rock geology model.

Fig. 9:

The prestack migration image from the 2D hard rock geology model. Actual velocity model is overlaid onto the migrated section.

Fig. 10:

Kirchhoff PSTM image from the 2D hard rock synthetic model. Migration velocities from the presented migration were used as an input velocity model.

Fig. 11:

Kirchhoff PSTM image from the 2D hard rock synthetic model. Migration velocities from the presented migration were used as an input velocity model. Actual velocity model is overlaid onto the migrated section.

Fig. 12:

2D stacking velocity model, which was obtained from a velocity analysis after applying DMO corrections.

Fig. 13:

Kirchhoff PSTM image from the 2D hard rock synthetic model. Stacking velocities from the velocity analysis were used as an input velocity model.

Fig. 14:

Kirchhoff PSTM image from the 2D hard rock synthetic model. Stacking velocities from the velocity analysis were used as an input velocity model. Actual velocity model is overlaid onto the migrated section.

EQUATIONS

$$x_m = x_s - (x_r - x_s)p_s \frac{t-(x_r-x_s)p_r}{t(p_r-p_s)+2(x_r-x_s)p_s p_r}, \qquad (1)$$

$$V^2 = \frac{x_s-x_m}{tp_s} + \frac{x_r-x_m}{tp_r}, \qquad (2)$$

$$t_0 = \frac{|x_s-x_m|}{V}\frac{\sqrt{\frac{1}{V^2}-p_s^2}}{|p_s|}, \qquad (3)$$

where V is the migration velocity, t_0 is the vertical travel-time, x_m is the horizontal coordinate of the migrated reflection point, p_r and p_s are values of horizontal slownesses measured in common-shot and common-receiver gathers respectively, x_s and x_r are the locations of source and receiver, t is the travel-time of the migrated event.